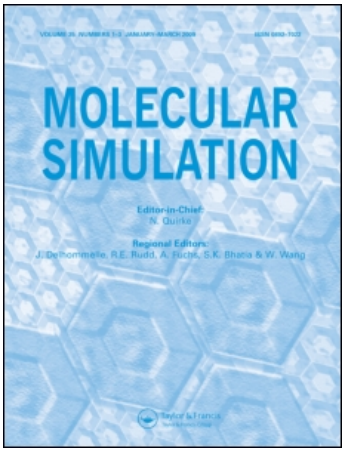

Molecular Simulation
Publication details, including instructions for authors and subscription information:
http://www.informaworld.com/smpp/title~content=t713644482

Molecular Dynamics Simulation of the Human Apo-dihydrofolate Reductase: An Investigation of an Unstable Enzyme

Pornthep Sompornpisut[a]; Atchara Wijitkosoom[a]; Vudhichai Parasuk[a]; Worachart Sirawaraporn[b]
[a] Department of Chemistry, Faculty of Science, Chulalongkorn University, Bangkok, Thailand [b] Department of Biochemistry, Faculty of Science, Mahidol University, Bangkok, Thailand

Online publication date: 26 October 2010

To cite this Article Sompornpisut, Pornthep , Wijitkosoom, Atchara , Parasuk, Vudhichai and Sirawaraporn, Worachart(2003) 'Molecular Dynamics Simulation of the Human Apo-dihydrofolate Reductase: An Investigation of an Unstable Enzyme', Molecular Simulation, 29: 2, 111 — 121
To link to this Article: DOI: 10.1080/0892702031000065782
URL: http://dx.doi.org/10.1080/0892702031000065782

Molecular Simulation, 2003 Vol. 29 (2), pp. 111–121

Molecular Dynamics Simulation of the Human Apo-dihydrofolate Reductase: An Investigation of an Unstable Enzyme

PORNTHEP SOMPORNPISUT[a,*], ATCHARA WIJITKOSOOM[a], VUDHICHAI PARASUK[a] and WORACHART SIRAWARAPORN[b]

[a]*Department of Chemistry, Faculty of Science, Chulalongkorn University, Phayathai Road, Bangkok 10330, Thailand;* [b]*Department of Biochemistry, Faculty of Science, Mahidol University, Bangkok 10400, Thailand*

(Received April 2001; In final form July 2001)

Structure and dynamics data of the *Homo sapiens* apo-dihydrofolate reductase (hDHFR) have been investigated by molecular dynamics (MD) simulation. The MD simulation for a total of 300 ps was performed for the system containing the apo-hDHFR with explicit water molecules. The last 250 ps MD trajectory of the equilibrated system was generated and the 25 sampling structures of the apo-hDHFR were analyzed. The statistical quantities of the simulation reveal significant differences between the apo-enzyme and the complex form. The differences include the mainchain mobility, the solvent accessibility, the secondary structures, the phenylalanine movement and the hydrogen bond may relate to the stability of the enzyme. The tertiary folding from the secondary structure motif reveals a less compact for the apo-enzyme structure with respect to the X-ray structure of the hDHFR-folate complex. In addition, intramolecular hydrogen bond involving the backbone protons dramatically decreases. Comparisons between the unbound and the ligand-bound enzyme obtained from the X-ray, NMR and MD data are discussed.

Keywords: Molecular dynamics; Dihydrofolate reductase; Apo-enzyme; Root mean square deviation

1. INTRODUCTION

Knowledge of the structure and dynamics of biological macromolecules at an atomic level is essential for understanding their functional mechanism in biochemical process. To reach such fundamental relationship, molecular dynamics (MD) calculations have considerably become one of the powerful techniques for investigating dynamics information from atomic coordinates [1,2]. This computational tool provides structural statistics that link to its biological task in physiological conditions. This technique has also great potential to extend details that the experimental observations are missing due to technical difficulty or impracticality. The MD applications have successfully revealed the structure-function relationship for numerous proteins, including the enzyme dihydrofolate reductase (DHFR:E.C.1.5.1.3).

DHFR has been a remarkable attention in molecular and structural research because of its biological and clinical importance. DHFR is a crucial enzyme responsible for the biosynthesis of nucleotide in living organisms. The biological role of this enzyme is to catalyze the NADPH-dependent reduction of 7, 8-dihydrofolate or folate to 5,6,7,8-tetrahydrofolate required in several biochemical processes including biosynthesis of thymidylate, purines, and certain amino acids. For the clinical usefulness, DHFR has been significantly useful as a drug target of antifolate inhibitors for a number of diseases. This includes anticancer (methotrexate, MTX), antibacterial infection (trimethoprim, TMP) and antimalaria (pyrimethamine, PYR) and cycloguanil, CYC), etc [3].

Because of the appropriate size of the enzyme molecule (15–30 kD), it is, therefore, amenable for the structural study using X-ray crystallography and NMR spectroscopy. The three-dimensional structures of the DHFR wildtype and the drug resistant

*Corresponding author. Address: Department of Chemistry, Faculty of Science, Chulalongkorn University, Bangkok 10330 Thailand. Tel.: 662-2185224. Fax: 662-2541309. E-mail: spornthe@chula.ac.th

ISSN 0892-7022 print/ISSN 1029-0435 online
DOI: 10.1080/0892702031000065782

mutants in protozoal, bacterial and vertebrate DHFRs have been reported. These include *Leishmania major* [4], *Lactobacillus casei* [5,6], *Escherichia coli* [5,7,8], *Pneumocystis carinii* [9], chicken liver [10–13] and human [14–16]. The atomic coordinates of those DHFR structures have shown that the tertiary folding pattern of the enzyme is similar and the secondary structures are very well conserved. Despite the similarity of their overall folding topology, subtle differences do exist, particularly residues surrounding the substrate-binding site. Such differences are crucial for enzyme selectivity and specificity to small organic molecules such as the substrate or antifolate inhibitors [17]. This requires atomic details associated with the dynamics information in order to design and develop novel and more effective inhibitors.

Most of DHFR studies reported so far were conducted in the presence of small ligand molecules such as the folate substrate or antifolate inhibitor. The fact is that the binary or the ternary enzyme complexes are the most interest for studying the protein-ligand interactions. Moreover, the binding of these small molecules is strong enough to stabilize the enzyme throughout experimental measurements. Without the substrate/inhibit or, many experimental techniques seem to fail due to protein instability [18]. What causes the enzyme in the absence of ligands to be unstable? Are there any conformational changes that could lead the apo-enzyme to unfold?

Here, we have performed the MD simulation of the apo-enzyme DHFR from *Homo sapiens* (hDHFR) in aqueous solution at 300 K, with the objectives (1) to obtain dynamics information of the apo-enzyme; (2) to extend the knowledge of the crystal structure of the human DHFR; (3) to relate some specific properties of the calculation to experimentally observable quantities for the system and (4) to find out possible evidence influencing the stability of the enzyme. The hDHFR is a monomeric protein consisting of 186 amino acid residues (21.5 kD) that make possible to pursuing MD study with a timescale of hundreds picosecond. Its 3D crystal structures with the resolution ranging from 2.0 to 2.5 Å have been solved by the X-ray diffraction techniques. The resonance assignments of the backbone and the side-chain protons of the hDHFR complexed with methotrexate in aqueous solution were achievable using multidimensional NMR spectroscopy. The NMR structure of the hDHFR-MTX-NADPH complex has been obtained from NOEs restraints around protein-ligand binding region [19]. Due to the poor stability of the apo-hDHFR, it is therefore not possible for structural studies through X-ray and NMR techniques. Availability from the X-ray and NMR data of the hDHFR complex is helpful for the purpose of comparison with the MD results.

2. COMPUTATIONAL DETAILS

The single crystal structure (Fig. 1) of the mammalian DHFR complexed with the folate refined at 2.0 Å resolution [14] was taken from the Brookhaven Protein Data Bank (http://www.rcsb.org and pdb ID: 1drf). The structure was then used as the starting conformation of the study. The atomic coordinates belonging to the folate, water and sulfate molecules were removed. In order to obtain the full protein structure, the missing sidechain atoms of Gln12 were built on the basis of the internal coordinates of glutamine residue in the Amber amino acid library. Addition of hydrogen coordinates was considered the ionization-state of the charged residues including Glu, Asp, Arg and Lys as well as the positive and negative charges at N-terminal Val1 and C-terminal Aspl86. Energy minimization of the hDHFR molecule was subsequently performed to improve the poorly defined regions present in the protein structure as a consequence of the geometrically inappropriate construction of added atoms.

All energy calculations were conducted using the Cornell *et al.* all-atom force field model available in the program Amber [20]. The steepest descent algorithm was applied through the first 5000 steps and then followed by the conjugated gradient algorithm for the remaining minimization. The convergence criterion of 1.0×10^{-4} kcal mol^{-1} Å^{-1} was chosen for the energy gradient otherwise the maximum minimization step is reached. The treatment of

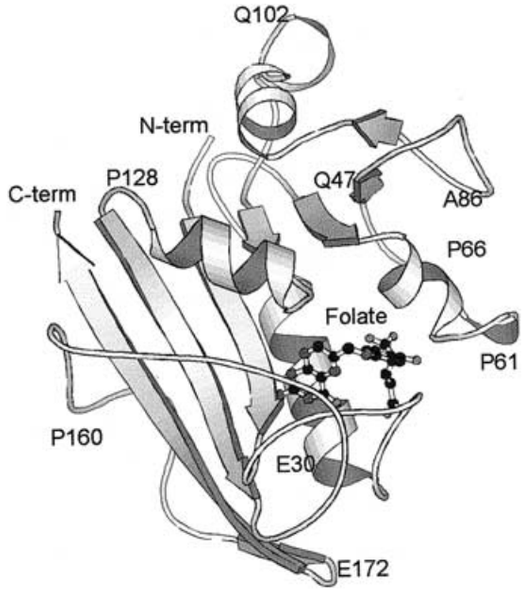

FIGURE 1 Schematic representation of the X-ray structure (1drf) showing the secondary structure elements and the substrate folate. The figure was generated using MOLSCRIPT [27].

TABLE I Relevant simulation parameters for the MD simulation

Protein-solvent simulation condition	*Simulation data*
Energy minimization	
In vacuo	60,000 steps (5,000 steps steepest descent and 55,000 conjugated gradient)
In water	60,000 steps (5,000 steps steepest descent and 55,000 conjugated gradient)
Molecular dynamics	
Number of atoms	19933 (atoms) 3013 protein atoms and 5640 TIP3P water molecules
Thermodynamic ensemble	Isobaric-isothermal ensemble (NPT)
Integration algorithm	Leapfrog
Integration time step	0.001 ps
Constraints	No
Long-range interactions	10 Å residue cut off distance
Periodic boundary conditions	Box dimension $64.8 \times 57.6 \times 52.8\,\text{Å}^3$
Thermalization	15 ps
Equilibration	35 ps
Dynamics trajectory for structural evaluation	250 ps
Collection of coordinate sets	2500 substructures (every 0.1 ps)

long-range electrostatic interactions was employed by a residue-based cutoff value of 10.0 Å.

The energy-minimized coordinates were placed afterwards in a rectangular box of water. To employ the method of periodic boundary conditions, the cubic dimension of $64.8\,\text{Å} \times 57.6\,\text{Å} \times 52.8\,\text{Å}$ was defined with a total of 19933 atoms, including 3013 protein atoms solvated by 5640 explicit water molecules. This represents sufficient numbers of solvent molecules as to make the results obtained meaningful. The interactions involving the solvent molecules were modeled by the well-known three-center charge TIP3P model [21]. Since the simulation of this step was carried out in the explicit solvent water molecules, the dielectric constant of 1 was used. The periodic boundary conditions were employed throughout the simulations. Another energy minimization of the protein in aqueous solution was performed.

The MD simulation was carried out in subsequent calculations. An isobaric-isothermal ensemble (NPT) was employed using constant pressure of 1 atm and constant temperature of 300 K. The pressure was kept constant by coupling to an external pressure bath [22] with a coupling constant of 0.2 ps. The velocities of the atoms were assigned according to a Maxwellian velocity distribution at 300 K. The integration of the equation of motion was done using a leapfrog algorithm employing the time step of 1 fs. For the first 50 ps of the MD simulation, an equilibration of the protein in solution was reached after warming up the system for 15 ps. During the thermalization period, the temperature was adjusted with the SHAKE option using the Berendsen coupling algorithm. A single scaling factor was used for all atoms at 300 K. A set of the coordinates containing enzyme structure with bulk solvent water molecules, so called MD trajectory, was collected every 0.1 ps over the last 250 ps and was used to monitor the dynamics behavior of the simulation. The overall behavior of the MD simulation was analyzed by assessments of the fluctuation of total energy, kinetic energy, potential energy, pressure, volume, temperature of the solution and the deviation of the atomic positions (or a root-mean-square deviation, RMSD) as a function of time. RMSD calculation for hDHFR did not take into consideration the effect of the N- and C-terminal, neglecting the first and the last three residues. Relevant simulation parameters were summarized in Table I. All MD simulation and analysis of MD trajectory were performed using the program Amber 5 [23]. The three-dimensional structures were visualized using the program Swiss-PdbViewer [24], Rasmol [25], Molmol [26] and Molscript [27]. Evaluation of the quality of the protein structure was performed using Procheck [28]. The simulations were performed on an SGI Power Challenge XL 8 × R10000.

3. RESULTS AND DISCUSSION

3.1. Energy Minimization

The energy minimization profiles of the apo-enzyme hDHFR in the absence of water molecules reveal a rapid drop from $4.60 \times 10^3\,\text{kcal mol}^{-1}$ to $-6.0 \times 10^3\,\text{kcal mol}^{-1}$ and then insignificantly alter. The final potential energy of the minimized enzyme structure was $-6.17 \times 10^3\,\text{kcal mol}^{-1}$. The potential energy of the system containing the apo-enzyme and water molecules starts with $-5.33 \times 10^4\,\text{kcal mol}^{-1}$ and reached a value of $-7.82 \times 10^4\,\text{kcal mol}^{-1}$ when minimized. The energy profile curves of the apo-enzyme both in the presence and absence of water were similar, implying that the minimization significantly decreased the strain of the system.

The system was gradually relaxed and ready to perform MD simulation for the next investigation.

3.2. Molecular Dynamics

3.2.1. Analysis of the MD Trajectory

In a molecular dynamics simulation, the trajectory of coordinates of hundreds picosecond provides useful information that some statistical quantities can be extracted. Figures 2A and B illustrates the energy profiles (total energy, kinetic energy, potential energy) and temperature of the simulated system for 300 ps, respectively. As a typical MD simulation, the results are well behaved. We observed rapid initial equilibration and slight fluctuations over a longer simulation time scale. The overall MD profiles obtained were most common to those observed in other protein simulations [29,2]. Analysis of properties of the system performed after the first 50 ps and the final MD parameters averaged over the last 250 ps are summarized in Table II.

TABLE II The average values from the MD simulation

MD parameters	*Mean values*
Total energy ($\times 10^4$ kcal mol^{-1})	-4.83 ± 0.009
Kinetic energy ($\times 10^4$ kcal mol^{-1})	1.26 ± 0.006
Potential energy ($\times 10^4$ kcal mol^{-1})	-6.09 ± 0.011
Temperature of the enzymes (K)	301 ± 4

For the last 250 ps of the MD trajectory, the apo-hDHFR coordinates of all collected configurations were used to generate an average structure, which is in turn used to calculate the RMSD of atomic coordinates. Figure 2C shows a plot of the mean global RMSD with respect to the ensemble average structure versus the simulation time of 250 ps. The RMSD for backbone atoms of residues Ser3-Glu l83 over the MD trajectory was in a range of 0.50–0.90 Å. This structural fluctuation is not uncommon in the typical MD simulation of protein, indicating the reliable equilibration of the system in this study.

3.2.2. Sampling Configurations and Evaluation

A set of 25 snapshot structures taken every 10 ps from the 250 ps MD trajectory is shown in Fig. 3A. A superposition of the 25 substructures manifests the mean global RMSD of 1.38 ± 0.17 Å for the backbone atoms and 1.72 ± 0.15 Å for the heavy atoms. As shown in Fig. 3B, the conformations of 25 MD structures superimposed on each other were considerable similar. Three segments with the largest

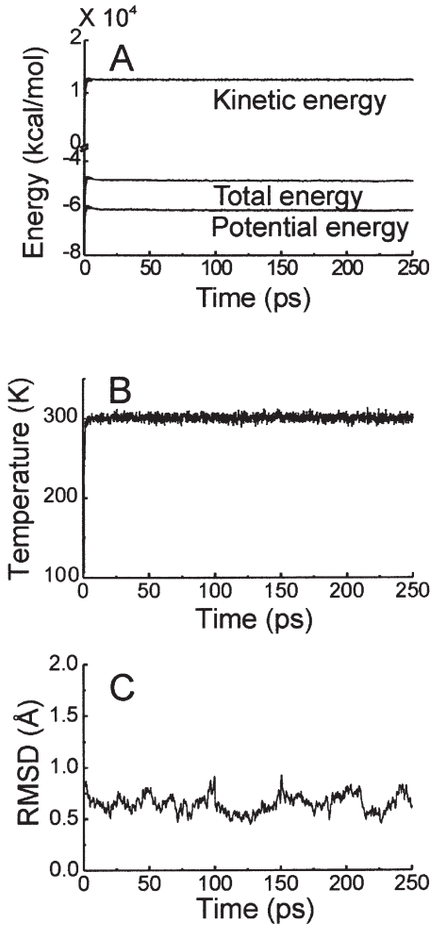

FIGURE 2 MD simulation profiles for the total energy, the potential energy, the kinetic energy (A), the temperature (B), the mainchain fluctuation of the enzyme with respect to that of the average energy-minimized structure (C).

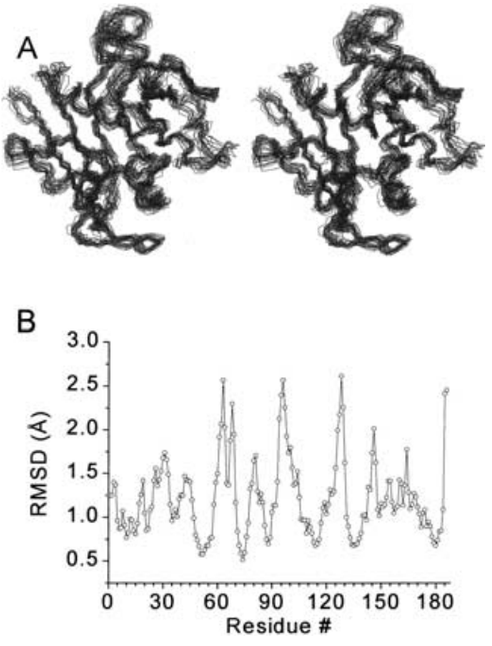

FIGURE 3 Stereo views showing the backbone α-carbon of the hDHFR (A) and its corresponding RMSD (B). The structures were taken every 10 ps from the MD trajectory. The figure was prepared with the program MOLMOL [26].

backbone fluctuation (RMSD > 2.0 Å) encompass residues Glu62-Asn64, Asp94-Leu97 and His 127-Gly129.

The 25 MD sampling configurations were evaluated. The calculation of mainchain torsion angles of the apo-hDHFR showed that no geometrically distortion of the backbone polypeptide was found, except for Ser 118. The backbone dihedral angles, ϕ and ψ, of the apo-enzyme fall within the structurally favorable regions of Ramachandran diagram. This is an indication of a good quality of regular protein structures.

The elements of the protein secondary structure were computed using the DSSP algorithm [30]. The tertiary folding and secondary structure elements of the solvated apo-hDHFR are mostly comparable to that of the hDHFR-folate complex in the crystallographic state. Significant discrepancy between the X-ray diffraction and the MD calculations was found for the two secondary structures as follows: the β-strand (Phe88-Ser90) and the short α-helical structure (Pro6l−Arg65). From the 25 configurations sampling from the MD trajectory, the β-strand changed to a coil structure, while the disruption of the α-helix was observed with 65% occurrence. Among the known 3D structures of DHFR family including from *L. casei*, *E. coli*, chicken liver, *P. carinii* and *L. major*, the strand is one of the seven conserved β-structures while the helix is not. Interestingly, these two regions are short in numbers of residue and close in contact with the bulk solvent. Perhaps these two segments involve in the early event of denaturation of the mammalian apo-enzyme.

3.2.3. Mobility from RMSD and the Solvent Accessibility

In this study, the RMSD was used to indicate the local movement along the mainchain polypeptide relative to the molecular tumbling rate in solution. The RMSD values for the backbone atoms of the 25 sampling coordinates were thus characterized the amino acid residues into three categories: immobilized to slightly mobile residue (for residues RMSD < 1.0 Å); fairly mobile residue (1.0 Å $\leq$ RMSD ≤ 2.0 Å); and very mobile residue (RMSD > 2.0 Å). From the simulation, each category was composed of 36, 56 and 8% amino acids from a total of 186 residues, respectively.

It should be noted that the highly mobile residue has the greatest potentials of the conformational perturbation in the absence of the cofactor of the enzyme. Residues of the third category are, therefore, of interest because they may involve either the protein-ligand contact or the denaturing event or both. It should, however, be careful to not over-interpret the results of hundreds picosecond timescale. In addition, the residue experiencing rapid conformational movement is typically located at the protein surface. As can be seen (Fig. 3), this category composes of residues present in the helical structures (Glu62-Asn64 and Asp94-Leu97) and in random coil segments (Lys68, His127-Glyl29, Thrl46). Most of these residues are solvent exposed.

It is obvious that a hydrophilic residue that is exposed to the protein surface has more favor of the conformational mobility, thus raising the RMSD value. To analyze this more quantitatively, the solvent accessible surface area (SASA) was computed using an algorithm developed by Connolly [31] with the probe radius of 1.4 Å. The total SASA values of all 25 MD sampling structures were approximately 10% higher than that of the crystal structure. Here a term called "the solvent accessibility (SA)" was defined as the calculated SASA divided by a total surface area of a residue being considered. A higher value of SA of a residue, the more chance of residue interacts to the solvent. For instance, if the SA value of a residue is 0 (dimensionless), this residue is completely buried. It is unlikely that the solvent molecule can contact to the residue. Figure 4A shows a plot of the average SA per residue obtained from the accessibility calculation of the 25 MD structures. Distribution of the SASA values (Fig. 4A) of all residues reveals the protein is compact. Most residues are embedded in the protein. About 50% of residues are below 0.2 of the SA value (Fig. 4B). However, Fig. 4C is a plot of the difference of the solvent accessibility (ΔSA) between the average 25 MD structures and the X-ray structure along the entire sequence. Apparently, most residues of the solvated apo-enzyme have positive ΔSA, suggesting a more contact to the environment with respect to those of the crystal structure.

3.2.4. Comparison to the X-ray Structure

We have so far discussed the comparisons of the tertiary and secondary structures and the accessibility between the free enzyme in the aqueous environment and the folate bound enzyme in the crystal structure. In order to determine the magnitude of the MD structures drifted from the crystal coordinates, RMSD calculation was performed using the reference X-ray structure and the 25 sampling structures of the MD simulation. This comparison may indicate conformational differences between the bound (hDHFR-folate) and free (apo-hDHFR) enzyme. The global RMSD per residue and the superposition structures between the X-ray hDHFR-folate and the 25 structures apo-hDHFR are shown in Fig. 5. The RMSD values suggest a significant

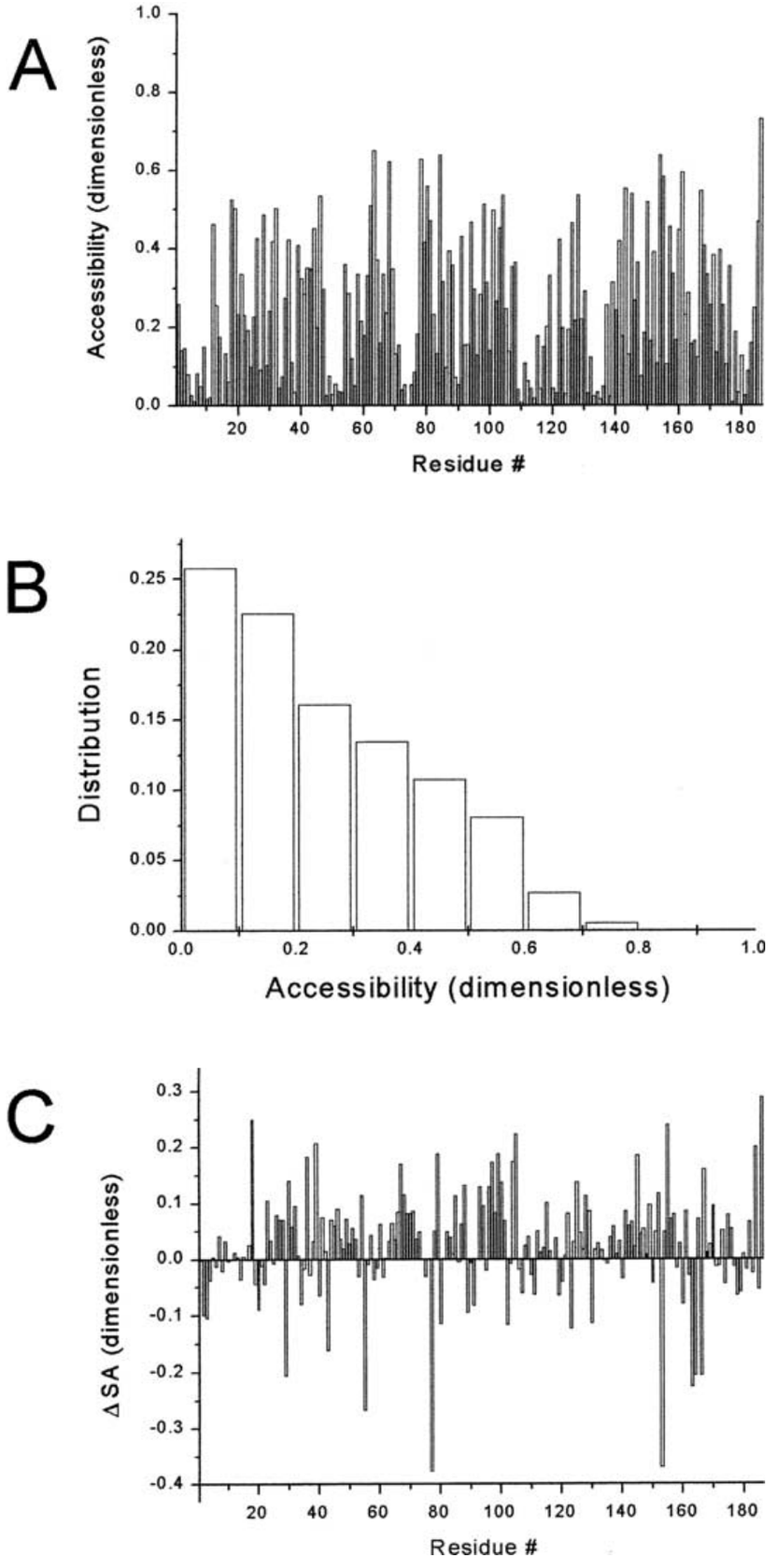

FIGURE 4 The solvent accessibility per residue (A), the residue, distribution of the accessibility (B), and the accessibility difference between the MD and the X-ray structures (C). The solvent accessibility was calculated with the program MOLMOL.

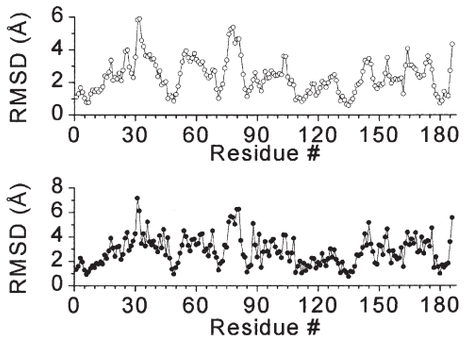

FIGURE 5 RMSD per residue of the 25 MD structures with respect to the X-ray structure: for the backbone atoms (A) and for the heavy atoms (B).

difference between the two structures (2.64 Å for the backbone atoms and 3.20 Å for the heavy atoms). Despite the similar folding patterns between the X-ray and the average structure, the RMS differences of some residues are sizeable to reflect the conformational differences. In this study, the backbone RMSDs of residues Pro26, Phe3l-Phe34, Ser76-Glu8l, and Glyl64 were in a range of 4–6 Å. Interestingly, residues Phe31-Phe34 are located within 5 Å accounting from the folate coordinates.

In the unbound state, the residues surrounding the binding site may possess a more rapid conformation movement with respect to that in the complex form. This results in an increase of the mainchain mobility. From an observation of six isomorphous crystallographic structures of *E. coli* DHFRs, the loop and domain motions were influenced by the folate and NADPH [32]. Such conformational rearrangements occur when the enzyme releases the folate product (http://chem-faculty.ucsd.edu/kraut/dhfr.html). From the X-ray structure of the folate-DHFR complex, 24 residues that are located within 5.0 Å accounting from the atomic coordinates of the folate were identified. These residues are summarized with the RMSD in Table III. Four out of the 24 ligand-encountered residues exhibiting the RMSD over 4.0 Å were located in the α-helix conformation. However, we remark on the possibility that there might be a considerable difference between both the conformations for the RMSD in a range of 3–4 Å.

Although the RMSD and SA values seem arbitrarily to relate with the experimental data, our data are consistent with the previous proposal from the crystallographic study of *E. coli* DHFR (ecDHFR). Structural invariance was commonly seen in the vertebrate DHFRs, while it is not for the case of bacterial DHFRs [32]. In ecDHFR, the loop and domain movements encompass Met16-Asn23 and His45-Trp47, respectively. The alignment residues Lys18-Pro25 and Lys55-Trp57 of the hDHFR that are homologous to these two segments

TABLE III Comparisons of RMSD and the solvent accessibility between the X-ray and the average MD structures. Residues with in 5 Å from the folate are reported

Residue	*RMSD* (Å)	
	Backbone	*Heavy*
Ile7	0.77	1.14
Val8	1.29	1.44
Ala9	1.52	1.65
Leu22	2.57	3.24
Arg28	2.56	3.26
Glu30	3.55	4.26
Phe31	5.85	7.19
Arg32	5.9	6.14
Tyr33	4.58	3.45
Phe34	4.2	4.27
Gln35	3.65	3.26
Thr38	3.43	3.35
Thr56	3.53	3.3
Ser59	3.79	3.83
Ile60	3.42	3.37
Pro61	3.28	3.46
Asn64	2.78	2.81
Leu67	2.38	3.31
Lys68	2.78	4.49
Arg70	1.59	2.33
Val115	1.48	1.65
Gly116	1.35	1.54
Val121	1.67	1.7
Thr136	0.82	1.18

were, however, slightly mobile (RMSDs within the ensemble were in a range of 0.7–1.4 Å). The RMSD values for the heavy atoms of this segment scattered between 2.2–3.9 Å. The SASA values calculated from the crystal structure of the ternary complex of ecDHFR were about twofold greater than those of human DHFR apo-enzyme. However, there is still inconclusive to explain why the mobility of the mammalian and the bacterial DHFRs are different.

3.2.5. Deviation of Aromatic Rings of Phenylalanine Side-chain

The dynamics information of the phenylalanine sidechain were extracted from the MD trajectory. As depicted in Fig. 6, we monitored the dynamics profile of phenylalanine rings (the χ_2 torsion angles of Cα–Cβ–Cγ–Cδ) along the 250 ps trajectory. The residues Phe58, Phe88, Phe134, Phel42, Phe147, Phel48 and Phel79 were also included in the analysis. The profiles indicated that the χ_2 values of most phenylalanine residues including Phe34, Phe58, Phel34, Phel42, Phel47 and Phe148 were between 80–100° or equivalent to −100–80° (because of the presence of the symmetry of the aromatic ring), with an average fluctuation of 20°, implying the similar orientation of the aromatic ring with respect to their Cα–Cβ-bond. A slight difference of the phenyl ring orientation was found for Phe88 and Phel79, of which the χ_2 values were around −120 and +120°, respectively. The sidechain of Phe3l exhibits the most

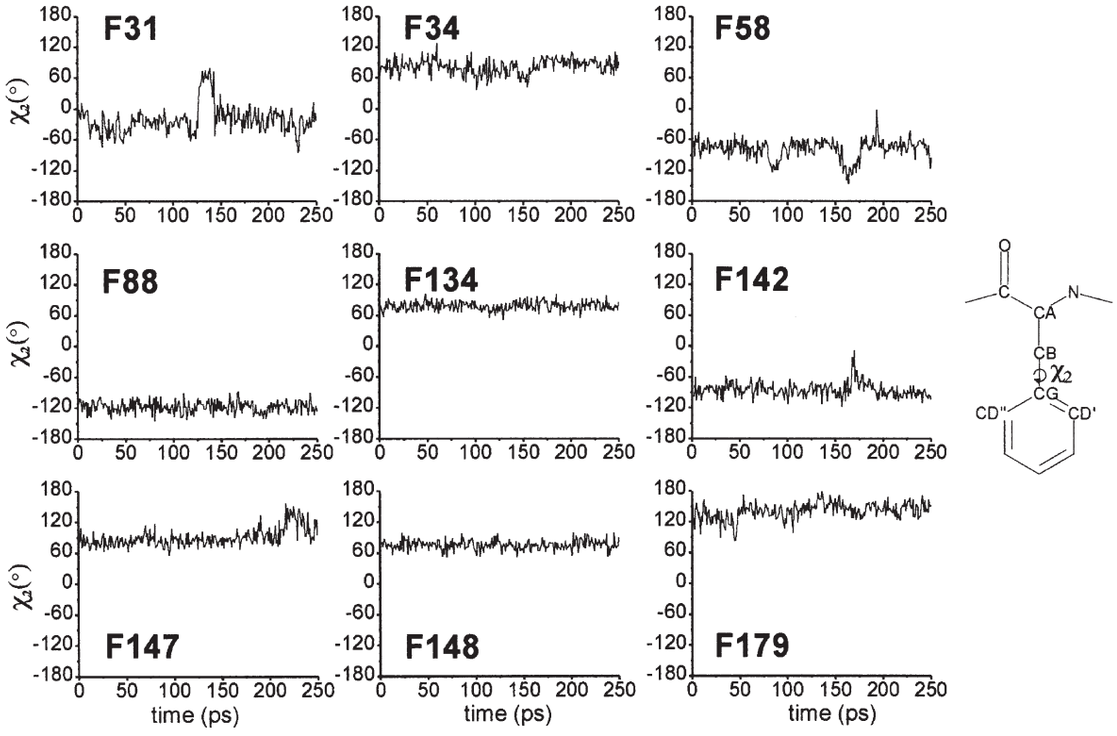

FIGURE 6 Dihedral angle χ_2 fluctuation of the sidechain of nine phenylalanines versus the period of the MD simulation.

different orientation as well as the fluctuation relative to the others.

According to the results from site-directed mutagenesis experiments, Phe3l and Phe34 of the wild-type protein, were previously reported to play a critical role for the binding efficiency of the ligand in the enzyme catalysis [33,34]. In the binary and ternary complexes of hDHFR, the phenyl ring of Phe34 forms a pi−pi stacking with the pteridine ring of the folate, but such interaction was unlikely in the case of Phe31 (Fig. 7). In the deficiency condition of the folate, the movement of aromatic ring of the side chain of Phe3l and Phe34 might relate to the conformational change of the apo-enzyme. From Fig. 6A, the flipping of the Phe3l ring was clearly observed and hence the most sensitive residue with respect to the others. The χ_2 value changed from -30 to $+60°$ and stabilized for a period of 30 ps and returned back again to the original equilibrium value. In contrast, χ_2 of Phe34 suggested only a minor movement of the side chain. The differences in orientation and the movement of the side chain between Phe31 and Phe34 in the apo-enzyme were likely affected by the unoccupied space in the binding pocket. It appears that there is a strong relationship between the mobility of the sidechain and the surface area of molecular contact. Phe34 is considerably buried in the protein with a low solvent accessibility (0.07) whereas the SA of Phe3l was 0.42 (Fig. 4A).

3.2.6. Comparison of Interamolecular Hydrogen Bond

It has been known that the effect of the interresidue hydrogen bond network plays an important role in folding and stabilizing protein conformations. Here,

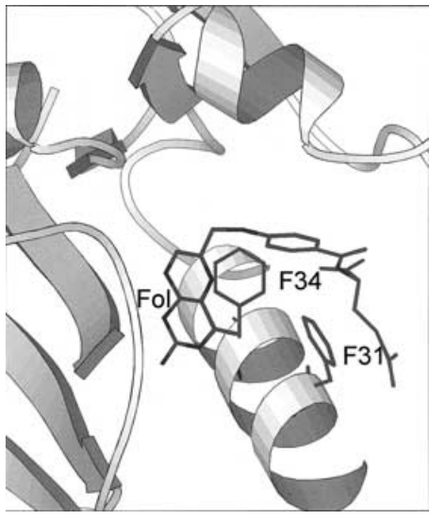

FIGURE 7 Schematic representation showing an orientation of Phe31, Phe34 and the folate in the X-ray structure. For clarification, some segments of the protein were not shown.

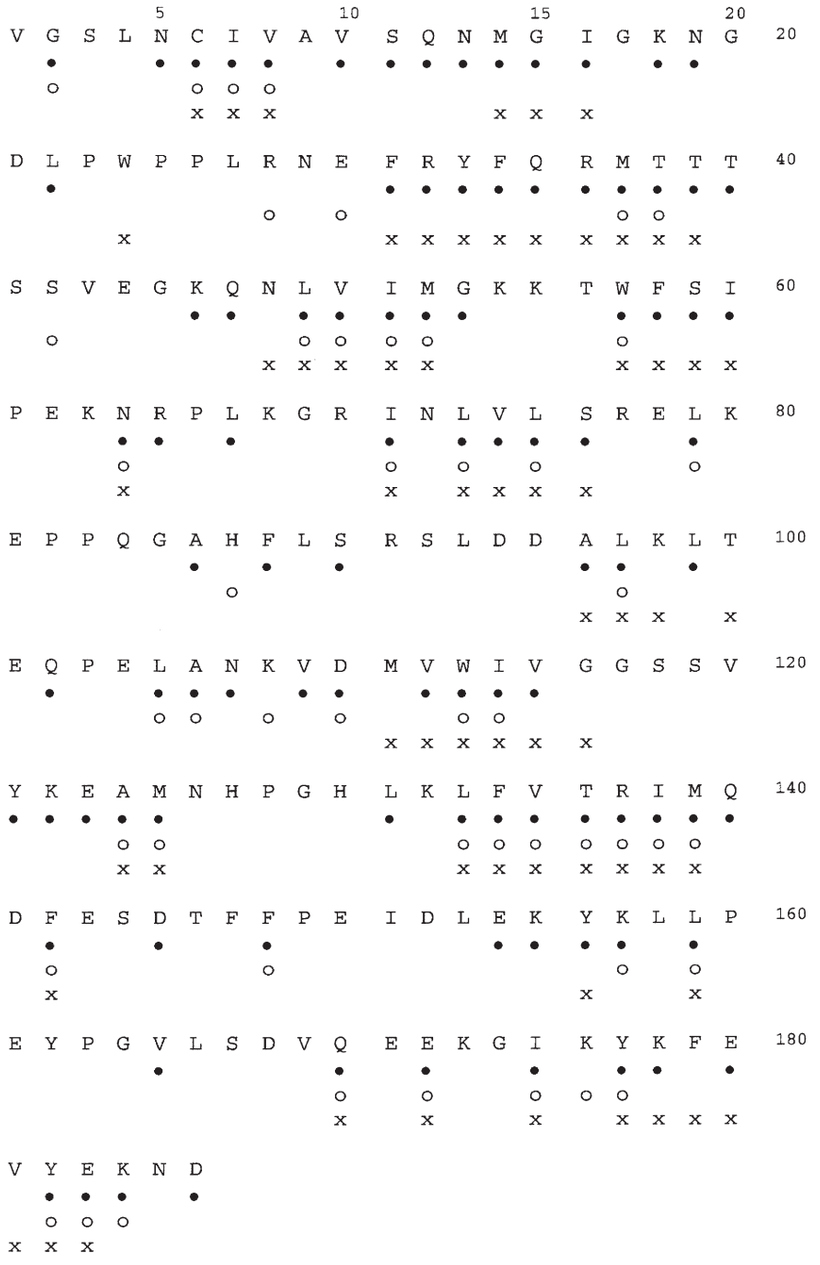

FIGURE 8 Comparison of the hydrogen bond involving.the NH protons: (•) predicted from the X-ray structure, (○) calculated from the MD structures and (×) taken from the NMR data [18].

additional information from the dynamics trajectory was further investigated by identification of possible hydrogen bond involving backbone hydrogen atoms of the apo-hDHFR. A principle criteria used to identify a possible formation of the hydrogen bond are: (1) a distance between a HN atom and the hydrogen bond acceptor should be below 2.5 Å and (2) the angle of N–HN the acceptor should not exceed 35°. About 94 out of 174 backbone amide protons (excluding 12 prolines) were found in the X-ray structure (Fig. 8). On the other hand, analysis of the 25 MD structures shows that 48 NH protons appearing consistently more than 80% of the ensemble are capable of forming the intramolecular hydrogen bond. It should be noted that the resonance assignment from the homonuclear and heteronuclear NMR spectra of the hDHFR complexed with methotrexate (MTX) identified 63 NH protons corresponding to the slow exchangeable proton [18]. Almost half of backbone hydrogen bond disappears from the simulation. Indeed, the number of the hydrogen bond involved with the NH protons between the MD simulation of the apo-enzyme and the NMR data of the hDHFR-MTX complex is

significantly different. As can be seen from Fig. 8, many vanishing NH protons, particular in the conserved α-helix encompassing residue 32–39, are rather not used to maintain regular secondary structures. This might suggest the apo-enzyme is less compact and eventually unable to sustain the conformation without the ligand molecule. Perhaps, this causes the enzyme to be unstable without the ligand.

4. CONCLUSIONS

The present study demonstrates the dynamics structures of the apo-enzyme in the absence of ligand. The MD simulation provides a tendency of conformational changes from the crystal structure of the enzyme-folate complex to the apo-enzyme in aqueous solution. The changes including the secondary structure, the solvent accessibility, the mainchain mobility and the hydrogen bond could play a critical role that relate to the stability of the apo-enzyme.

Acknowledgements

Part of this work was supported by the Thailand Research Fund Rachadapisek Sompoj Endowment, and National Science and Technology Development Agency. Thanks to Dr Banci and Dr Bates for critical review of the manuscript.

References

[1] McCammon, J.A. and Harvey, S.C. (1987) Dynamics of Proteins and Nucleic Acids (Cambridge University Press, Cambridge).
[2] Brooks, C.L., K., M. and Pettitt, B.M. (1988) Protein: A Theoretical Perspective of Dynamic Structure and Thermodynamics (Wiley, Canada).
[3] Schweitzer, B.I., Dicker, A.P. and B., J.R. (1990) "Dihydrofolate reductase as a therapeutic target", *FASEB J.* **4**, 2441.
[4] Knighton, D.R., Kan, C.-C., Howland, E., Janson, C.A., Hostomska, Z., Welsh, K.M. and Matthews, D.A. (1994) "Structure and kinetic channelling in bifunctional dihydrofolate reductase-thymidylate synthase", *Nat. Struct. Biol.* **1**, 186.
[5] Bolin, J.T., F.D., J., Matthews, D.A., Hamlin, R.C. and Kraut, J. (1982) "Crystal structures of *Escherichia coli* and *Lactobacillus casei* dihydrofolate reductase refined at 1.7 Å resolution. I. General features and binding of methotrexate", *J. Biol. Chem.* **257**, 13650.
[6] Birdsail, B., F., J., Tendler, S.J., Hammond, S.J. and Roberts, G.C. (1989) "Dihydrofloate reductase: multiple conformations and alternative modes of substrate binding", *Biochemistry* **28**, 2297.
[7] Bystroff, C., O., S.J. and Kraut, J. (1990) "Crystal structures of *Escherichia coli* dihydrofolate reductase: the NADP+ holoenzyme and the folate.NADP+ ternary complex. Substrate binding and a model for the transition state", *Biochemistry* **29**, 3293.
[8] Bystroff, C. and J., K. (1991) "Crystal structure of unliganded *Escherichia coli* dihydrofolate reductase. Ligand-induced conformational changes and cooperativity in binding", *Biochemistry* **30**, 2227.
[9] Champness, J.N., A., A., Ballantine, S.P., Bryant, P.K., Delves, C.J. and Stammers, D.K. (1994) "The structure of Pneumocystis carinii dihydrofolate reductase to 1.9 Å resolution", *Structure* **2**, 915.
[10] Volz, K.W., M., D.A., Alden, R.A., Freer, S.T., Hansch, C., Kaufman, B.T. and Kraut, J. (1982) "Crystal structure of avian dihydrofolate reductase containing phenyltriazine and NADPH", *J. Biol. Chem.* **257**, 2528.
[11] Matthews, D.A., Bolin, J.T., Burridge, J.M., Filman, D.J., Volz, K.W. and Kraut, J. (1985) "Dihydrofolate reductase: the stereocheniistry of inhibitor selectivity", *J. Biol. Chem.* **260**, 392.
[12] McTigue, M.A., D., J.F., Kaufman, B.T. and Kraut, J. (1992) "Crystal structure of chicken liver dihydrofolate reductase complexed with NADP+ and biopterin", *Biochemistry* **31**, 7264.
[13] McTigue, M.A., D., J.F., Kaufman, B.T. and Kraut, J. (1993) "Crystal structures of chicken liver dihydrofolate reductase: binary thioNADP+ and ternary thioNADP+biopterin complexes", *Biochemistry* **32**, 6855.
[14] Oefner, C., D., A.A. and Winkler, F.K. (1988) "Crystal structure of human dihydrofolate reductase complexed with folate", *Eur. J. Biochem.* **174**, 377.
[15] Davies, J.F., Delcamp, T.J., Prendergast, N.J., A., V.A., Freisheim, J.H. and Kraut, J. (1990) "Crystal structure of recombinant human dihydrofolate reductase complexed with folate and 5-deazafolate", *Biochemistry* **29**, 9467.
[16] Cody, V., Galitsky, N., Luft, J.R., Pangborn, W., Blakley, R.L. and Gangjee, A. (1981) "Comparison of ternary crystal complexes of F31 variants of human dihydrofolate reductase with NADPH and a classical antitumor furopyrimidine", *Anti-Cancer Drug Des.* **13**, 307.
[17] Matthews, H.R., Matthews, K.S. and Opella, S.J. (1977) "Selectively deuterated amino acid analoguest syntesis, incorporation into proteins and NMR properties", *Biochim. Biophys. Acta* **497**, 1.
[18] Stockman, B.J., N., N., Wagner, G., Delcamp, T.J., De Yarman, M.T. and Freisheim, J.H. (1992) "Sequence-specific 1H and 15N resonance assignments for human dihydrofolate reductase in solution", *Biochemistry* **31**, 218.
[19] Johnson, J.M., Meiering, E.M., Wright, J.E., Pardo, J., Rosowsky, A. and Wagner, G. (1997) "NMR solution structure of the antitumor compound PT523 and NADPH in the ternary complex with human dihydrofolate reductase", *Biochemistry* **36**, 4399.
[20] Cornell, W.D., Cieplak, P., Bayly, C.J., Gould, I.R., Merz, Jr, K.M., Ferguson, Jr, D.M., Spellmeyer, Jr, D.C., Fox, Jr, T., Caldwell, Jr, J.W. and Kollman, Jr, P.A. (1995) "A second generation force field for the simulation of proteins, nucleic acid, and organic molecules", *J. Am. Chem. Soc.* **117**, 5179.
[21] Jorgensen, W.L., Chandrasekhar, J., Madura, J., Impey, R.W. and Klein, M.L. (1983) "Comparison of simple potential functions for simulating liquid water", *J. Chem. Phys.* **79**, 926.
[22] Berendsen, H.J.C., Postma, J.P.M., van Gunsteren, W.F., DiNola, A. and Haak, J.R. (1984) "Molecular dynamics with coupling to an external bath", *J. Chem. Phys.* **81**, 3684.
[23] Case, D.A., *et al.* (1997) AMBER 5 (University of California, San Francisco).
[24] Guex, N. and P., M. (1997) "SWISS-MODEL, and the Swiss-PdbViewer: an environment for comparative protein modeling", *Electrophoresis* **18**, 2714.
[25] Sayle, R. (1994) Rasmol 2.6 edit. (Biomolecular Structure Department, Glaxo Research and Development, Greenford, Middlesex, UK).
[26] Koradi, R., Billeter, M. and Wuthrich, K. (1996) "MOLMOL: a program for display and analysis of macromolecular structures", *J. Mol. Graph.* **14**, 51.
[27] Kraulis, P.J. (1991) "MOLSCRIPT: a program to produce both detailed and schematic plots of protein structures", *J. Appl. Crystallog.* **24**, 946.
[28] Laskowski, R.A., MacArthur, M.W., Moss, D.S. and Thornton, J.M. (1993) "PROCHECK: a program to check the stereochemical quality of protein structures", *J. Appl. Crystallog.* **26**, 283.
[29] McCammon, A.J., H.S., Ed. (1987) Dynamics of Proteins and Nucleic Acids (Cambridge university press, Cambridge UK).

[30] Kabsh, W. and Sander, C. (1983) "Dictionary of protein secondary structure; pattern recognition of hydrogen-bonded and geometrical features", *Biopolymers* **22**, 2577.
[31] Connolly, M.L. (1983) "Solvent-accessible surfaces of proteins and nucleic acids", *Science* **221**, 709.
[32] Sawaya, M.R. and Kraut, J. (1997) "Loop and sundomain movements in the mechanism of *Escherichia coli* dihydrofolate reductase: crystallographic evidence", *Biochemistry* **36**, 586.
[33] Chunduru, S.K., Cody, V., Luft, J.R., Pangborn, W., Appleman, J.R. and Blakley, R.L. (1994) "Methotrexate-resistant variants of human dihydrofolate reductase: effects of Phe3l substitutions", *J. Biol. Chem.* **269**, 9547.
[34] Nakano, T., Spencer, H.T., Appleman, J.R. and Blakley, R.L. (1994) "Critical role of phenylalanine 34 of human dihydrofolate reductase in substrate and inhibitor binding and in catalysis", *Biochemistry* **33**, 9945.